J. Iron Steel Res. Int. (2023) 30:1732–1742
https://doi.org/10.1007/s42243-022-00873-6

ORIGINAL PAPER

Distribution ratio of sulfur between high alumina slag and carbon-saturated iron

Shuai Wang[1] · Ying Jiang[1] · Yu-feng Guo[1] · Feng Chen[1] · Ling-zhi Yang[1] · Zhuang Yang[1] · Guang Li[1]

Received: 19 May 2022 / Revised: 19 September 2022 / Accepted: 20 September 2022 / Published online: 23 November 2022

Abstract

High alumina slag is widely found in pyrometallurgical extractions of ferronickel, ferrochromium, and platinum group metals. The effects of MgO, Al_2O_3, and CaO/SiO_2 on the sulfur distribution ratio between high-alumina $CaO–SiO_2–MgO–Al_2O_3$ slag and carbon-saturated iron were investigated. The slag consisted of Al_2O_3 content in the range of 27.61–40.00 wt.%, CaO/SiO_2 ratio of 0.8–1.1, and MgO content of 8–16 wt.%. The theoretical liquid areas of $CaO–SiO_2–MgO–Al_2O_3$ slag were analyzed through the phase diagrams. The sulfur distribution ratio was measured via the slag–metal equilibrium technique at 1500 °C. It was observed that the sulfur distribution ratio increased with higher MgO content and higher CaO/SiO_2 ratio largely due to the increase in free O^{2-} ions and the decrease in activity coefficient of sulfur ion in slag, but slightly decreased with the increasing Al_2O_3 content because of the decrease in free O^{2-}.

Keywords Sulfur distribution ratio · High alumina slag · Liquid area · Slag–metal equilibrium · Optical basicity

1 Introduction

There is an increasing demand for the production of low sulfur and ultra-low sulfur steel due to the competitive steel market [1–3]. The presence of high sulfur in steel affects the workability of steel, lowers hot ductility and toughness, and deteriorates welding properties [4–6]. About 90% of the metal produced in the blast furnace is desulfurized before it is sent to be processed in a steelmaking furnace [7]. Sulfide capacity (C_S) proposed by Fincham and Richardson [4, 8] and defined based on gas–slag equilibrium [9] is an effective concept to quantitatively characterize the removal of sulfur from metal. Previous researchers [10–12] also have used sulfide capacity to evaluate the desulfurization ability of slags based on slag–metal reactions due to the sulfide capacity of slag being related to the composition and temperature.

On the other hand, the use of lean ores leads to an increase in the Al_2O_3 content in slag, which deteriorates the physicochemical properties of the blast furnace slag and aggravates the difficulty of blast furnace operation. It can cause various problems, including poor fluidity of slag, larger volumes of slag, slag with a low desulfurization ability, difficulties in slag–iron separation, and a high smelting temperature [13–17]. Besides, high alumina slag is widely found in pyrometallurgical extractions of ferronickel, ferrochromium, and platinum group metals [18–20]. It is a general choice to increase the CaF_2 or FeO contents of high alumina slag to lower the melting point of the high alumina slag and enhance the kinetic efficiency of the desulfurization process [21–23]. However, these measures have been restricted and treated carefully due to the harmful effects of CaF_2 on human health and the significant iron losses caused by FeO. The effects of basicity, Al_2O_3, MgO, or other additives such as MnO and Na_2O on the properties of $CaO–SiO_2–MgO–Al_2O_3$ slag and desulfurization ability have been experimentally investigated by several researchers. Shankar et al. [24] reported that increasing CaO/SiO_2 ratio (C/S) from 0.70 to 1.25 and increasing MgO content from 5 to 7 wt.% can significantly improve the sulfide capacity of $CaO–SiO_2–MgO–Al_2O_3$ slag with more than 20 wt.% alumina. A similar result was obtained by Ma et al. [8] for the $CaO–SiO_2–MgO–Al_2O_3$ slag at fixed 15 wt.% Al_2O_3. Xu et al. [25] measured the melting temperature of the $CaO–SiO_2–MgO–Al_2O_3$ slag at

✉ Yu-feng Guo
yfguo@csu.edu.cn

[1] School of Minerals Processing and Bioengineering, Central South University, Changsha 410083, Hunan, China

fixed 7 wt.% MgO and the result indicated that the melting temperature decreased with the increase in the basicity from 2.08 to 4.87. Taniguchi et al. [26] also studied the sulfide capacity of $CaO–SiO_2–MgO–Al_2O_3$ slag and found that the desulfurization ability of slag increased with the increase in MgO content from 0 to 4 mass% and MnO content from 0 to 5 mass%. Van Niekerk and Dippenaar [27] reported that the sulfur distribution ratio (L_S) between carbon-saturated iron and $Na_2O–SiO_2–CaO$ slag significantly increased and the melting temperature decreased with the addition of Na_2O. Park and Min [28] found that Al_2O_3 decreased the sulfide capacity due to its acidic behavior.

In our study, to effectively enhance the desulfurization ability of high alumina slag, the sulfur distribution ratios between $CaO–SiO_2–MgO–Al_2O_3$ slag with high alumina and carbon-saturated iron were investigated. First, the effects of MgO, Al_2O_3, and CaO/SiO_2 ratio on the liquid areas and viscosities of the $CaO–SiO_2–MgO–Al_2O_3$ slag were predicted thermodynamically using FactSage 8.0 software. Then, their effects on the distribution ratio of sulfur between high alumina slag and carbon-saturated molten iron were measured via slag–metal equilibrium technique at 1500 °C. The microstructure and phases of desulfurization slag were analyzed through scanning electron microscopy-energy dispersive spectrometry (SEM–EDS) technique. Our study will provide a technical basis for the desulfurization in the high-temperature smelting process with high alumina slag.

2 Experimental materials and methods

2.1 Raw materials

The high alumina slag and cast iron used in the desulfurization experiment were provided by a steel company in China. The chemical composition of the cast iron sample is shown in Table 1. The slag samples in the experiments were half-synthetic slag. The designed amounts of analytical-grade reagents $CaCO_3$ ($\geq$ 98 wt.%), SiO_2 ($\geq$ 99 wt.%), MgO ($\geq$ 98 wt.%), and Al_2O_3 ($\geq$ 99 wt.%) were added to the high alumina slag to adjust the slag compositions. The chemical composition of the high alumina slag and the designed chemical compositions of the half-synthetic slags are shown in Tables 2 and 3. All reagents $CaCO_3$, SiO_2, MgO, and Al_2O_3 were roasted at 1000 °C for 1 h to remove carbonate and water. Each slag sample was uniformly mixed in an agate mortar for at least 30 min. The mass ratio of slag to metal was set as 0.6:1 according to industrial production.

2.2 Methods

The experimental method employed is based on the equilibrium between liquid metal and liquid slag to measure the sulfur distribution ratio. Initially, 20 g powdered cast iron and 12 g half-synthetic slags were added to a graphite crucible (30 mm in diameter and 60 mm in height) which was held on a corundum brick. The furnace was heated up to a target temperature at the rate of 10 °C/min. When the temperature in the furnace rose to 1500 °C, the corundum brick and the graphite crucible containing the samples were put into the furnace as shown in Fig. 1 and kept for 6 h when the temperature in the furnace reached 1500 °C again. The N_2 (> 99.99 vol.%) gas was introduced into the reaction tube to protect the samples and graphite crucibles from being oxidized in the whole heating process, with a flow rate of 3.5 L/min. When equilibrium was reached, the samples were taken out from the furnace and quenched into the cold water quickly. After being cooled, the iron was separated from the slag. The slag was dried and then crushed to less than 100 μm for chemical composition analysis. The iron was washed to remove surface residues. The sulfur contents of slag and iron were analyzed using a CS844 carbon–sulfur analyzer. The chemical composition of the slags was determined by chemical analysis methods. The sulfur distribution ratio of the slag is defined as $w_{(S)}/w_{[S]}$, where $w_{(S)}$ is the mass percentage of sulfur in slag, and $w_{[S]}$ is the mass percentage of sulfur in iron.

3 Results and discussion

3.1 Liquid areas of $CaO–SiO_2–MgO–Al_2O_3$ slag system

The FactSage software has been widely applied in the prediction of high-temperature processes with complex multi-component phase equilibria [29, 30]. Phase diagrams

Table 1 Chemical composition of cast iron (mass%)

C	Cr	Fe	Mn	Ni	P	S	Si
4.65	3.01	87.94	1.21	1.16	0.04	0.13	0.97

Table 2 Chemical composition of industrial blast furnace slag (mass%)

TFe	FeO	MFe	CaO	SiO_2	MgO	Al_2O_3	MnO	Cr	S
1.40	1.63	0.13	24.90	27.90	9.59	23.8	1.36	0.39	0.97

Table 3 Chemical composition of designed slag and calculation of theoretical melting temperature and viscosity (at 1500 °C) of slag

No.	Slag composition/mass%				CaO/SiO_2	Melting temperature/°C	Viscosity/(Pa s)
	CaO	SiO_2	MgO	Al_2O_3			
1	27.23	34.03	11.13	27.61	0.8	1524.0	1.99
2	29.02	32.24	11.13	27.61	0.9	1561.4	1.72
3	30.63	30.63	11.13	27.61	1.0	1585.4	1.49
4	32.09	29.17	11.13	27.61	1.1	1602.4	1.29
5	30.50	33.89	8.00	27.61	0.9	1454.3	2.00
6	26.71	29.68	16.00	27.61	0.9	1686.2	1.39
7	25.52	28.35	11.13	35.00	0.9	1658.6	2.96
8	23.15	25.72	11.13	40.00	0.9	1705.3	4.09

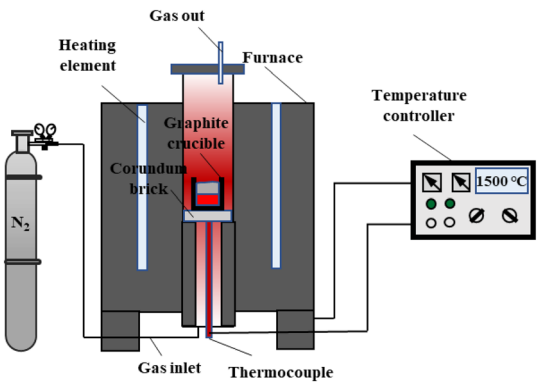

Fig. 1 Schematic view of experimental set-up for desulfurization

are crucial to understanding the correlation between the composition and thermodynamic properties of slags [5]. The phase diagrams were drawn by FactSage 8.0 software to predict the liquid areas of CaO–SiO_2–MgO–Al_2O_3 slag. The liquid areas of CaO–SiO_2–MgO–25 wt.% Al_2O_3 slag and CaO–SiO_2–10 wt.% MgO–Al_2O_3 slag for the temperature of 1300–2000 °C are shown in Fig. 2a, b. The effects of Al_2O_3 and MgO contents on the liquid areas of CaO–SiO_2–MgO–Al_2O_3 slag at 1500 °C are shown in Fig. 2c, d, respectively. As shown in Fig. 2, there are three dotted lines that represented the CaO/SiO_2 ratio of 0.8, 1.0, and 1.2, respectively. In CaO–SiO_2–MgO–25 wt.% Al_2O_3 slag system, when CaO/SiO_2 is constant, the melting point of the slag first decreases and then increases with the increase in MgO content. Similarly, in CaO–SiO_2–10 wt.% MgO–Al_2O_3 slag system, when CaO/SiO_2 is constant, the melting point of the slag first decreases and then increases with the increase in Al_2O_3 content. This supports the conclusion that the melting point of slag increased with increasing the basicity from 0.8 to 1.1, Al_2O_3 content from 27.6 to 40.0 wt.%, and MgO content from 8 to 16 wt.% in CaO–SiO_2–MgO–Al_2O_3 slag.

3.2 Reaction mechanism and sulfur distribution ratio

According to the two-film theory of the kinetic model for liquid–liquid phase reactions [31], the boundary layer characterizing the mass transfer resistance exists on both sides of the phase interface in the system consisting of molten metal and molten slag. The model of the desulfurization reaction between molten metal and molten slag is shown in Fig. 3. The desulfurization reaction can be described by the following steps:

(1) Sulfur diffuses from the molten metal to the slag–metal interface, and the concentration of sulfur is decreased as it moves from the slag phase to the interface. In the following equations, where [*M*] is the *M* element in the hot metal, (O) is the oxide or ions in the slag, respectively.

$$[S] \rightarrow [S]^* \quad (1)$$

(2) Interfacial chemical reaction takes place between sulfur and oxygen ion, and the monomeric sulfur is reduced and converted to sulfide.

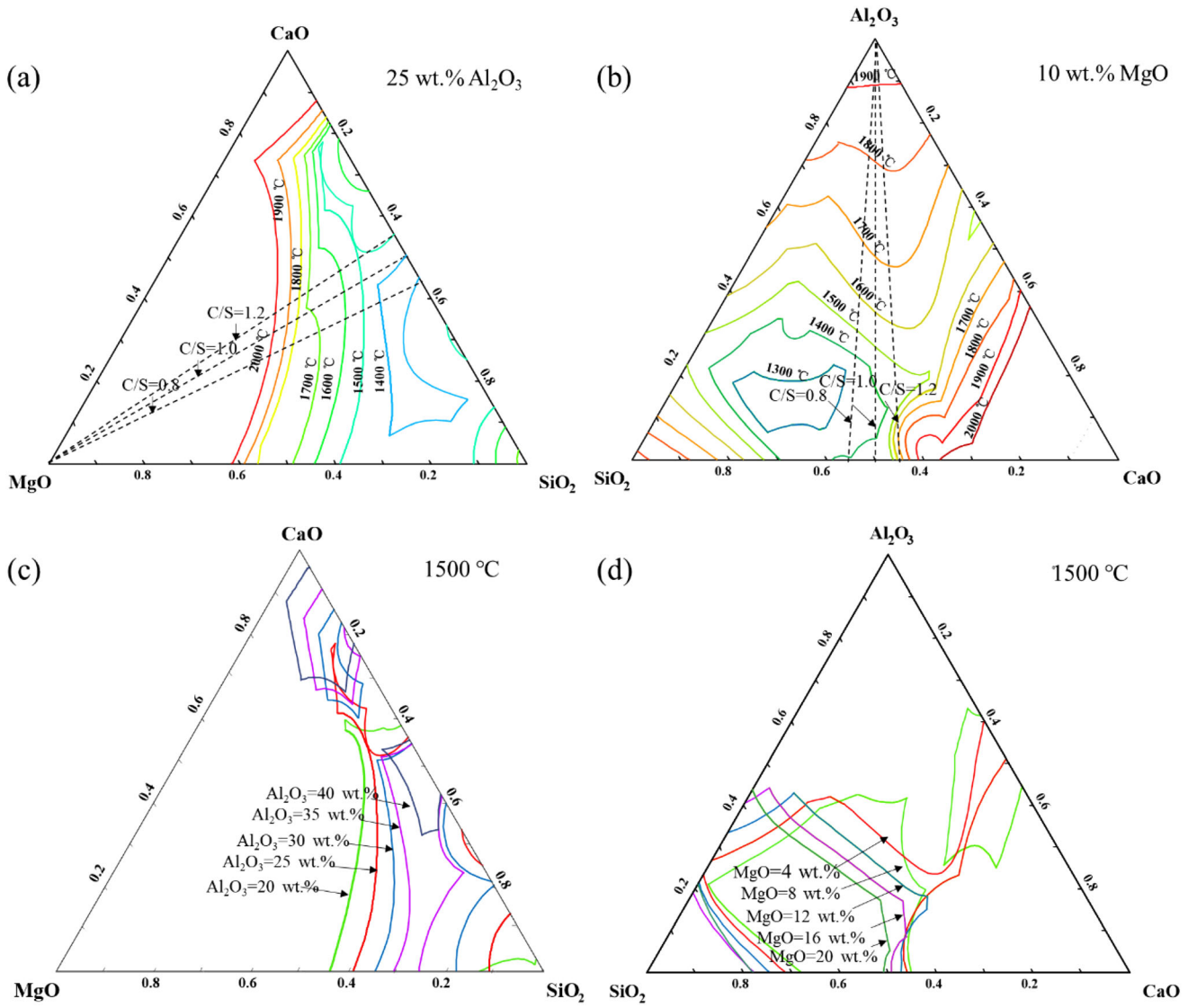

Fig. 2 Liquid areas of CaO–SiO_2–MgO–Al_2O_3 slag. **a** Liquid areas of CaO–SiO_2–MgO–25 wt.% Al_2O_3 slag with different temperatures; **b** liquid areas of CaO–SiO_2–10 wt.% MgO–Al_2O_3 slag with different temperatures; **c** effect of Al_2O_3 content at 1500 °C; **d** effect of MgO content at 1500 °C

$$[S] + (O^{2-}) = (S^{2-}) + [O] \quad (2)$$

(3) Generated sulfide diffuses from the interface into the slag, and the concentration of sulfide is decreased as it moves from the interface to the slag phase.

$$(S^{2-})^{*} \rightarrow (S^{2-}) \quad (3)$$

The sulfide capacity has been defined as Eq. (5) deduced from Eq. (4):

$$\frac{1}{2}S_2 + (O^{2-}) = (S^{2-}) + \frac{1}{2}O_2 \quad (4)$$

$$C_{S^{2-}} = w_{(S)} \cdot \frac{{P_{O_2}}^{1/2}}{{P_{S_2}}^{1/2}} = \frac{K_1 . a_{O^{2-}}}{\gamma_{S^{2-}}} \quad (5)$$

where $w_{(S)}$ is the mass percentage of sulfur in slag; P_{O_2} and P_{S_2} are the partial pressures of O_2 and S_2, respectively; K_1 is the equilibrium constant of reaction; $a_{O^{2-}}$ is the activity of oxygen in slag; and $\gamma_{S^{2-}}$ is the activity coefficient of sulfur ion in slag.

The equilibrium reaction of sulfur between slag and metal phases can be expressed as follows:

$$[S] + (O^{2-}) = [O] + (S^{2-}) \quad (6)$$

The sulfur distribution ratio between slag and metal can be related to sulfide capacity by incorporating Eqs. (4) and (6) as the following equation:

$$[S] + \frac{1}{2}O_2 = [O] + \frac{1}{2}S_2 \quad (7)$$

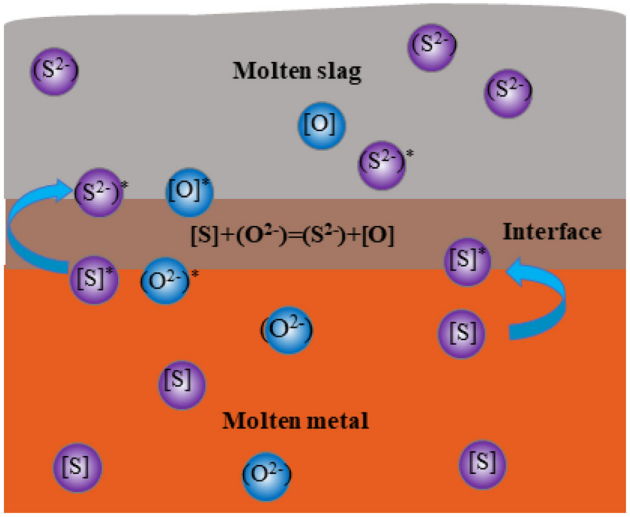

Fig. 3 Model of desulfurization reaction between molten metal and molten slag

For Eq. (7),

$$\log K_S = -\frac{935}{T} + 1.375 \tag{8}$$

$$K_S = \frac{a_O \cdot P_{S_2}^{\frac{1}{2}}}{a_S \cdot P_{O_2}^{\frac{1}{2}}} = \frac{a_O}{C_S \cdot f_S} \cdot \frac{w_{(S)}}{w_{[S]}} \tag{9}$$

where K_S is an equilibrium constant for reaction Eq. (7); f_S is the Henrian activity coefficient of sulfur in the hot metal; a_O and a_S are the activity of oxygen and sulfur in the hot metal, respectively; and T is temperature.

From Eqs. (8) and (9), the equilibrium sulfur partition ratio can be obtained as follows:

$$\log L_S = \log \frac{w_{(S)}}{w_{[S]}} = \log C_S - \log a_O + \log f_S - \frac{935}{T} + 1.375 \tag{10}$$

According to the Wagner model, the activity coefficient of sulfur or carbon in the hot metal can be obtained from Eq. (11):

$$\log f_i = \sum_i e_i^j \times w_{[j]} \tag{11}$$

where f_i is the activity coefficient of species i; e_i^j is the interaction parameter of species j on i; and $w_{[j]}$ is the concentration of species j in the hot metal, wt.%. The interaction parameters are given in Table 4.

The oxygen activity in the molten metal can be calculated by choosing the equilibrium of CO/C pairs, given in the following equation:

$$[C] + [O] = (CO)(g) \tag{12}$$

The equilibrium constant K_C for reaction (12) is as follows:

$$K_C = \frac{P_{CO}}{a_O a_C} \tag{13}$$

where P_{CO} is the partial pressure of CO.

The activity of carbon a_C can be calculated by

$$a_C = f_C \times w_{[C]} \tag{14}$$

The temperature dependence of the equilibrium constant is given by the following equation:

$$\log K_C = \frac{1.160}{T} + 2.003 \tag{15}$$

As shown in Fig. 3, the monomeric sulfur is reduced and converted to sulfide at the slag–metal reaction interface. Meanwhile, an equilibrium reaction of carbon and oxygen occurs as shown in Eq. (12). The overall atmosphere in the furnace is N_2, but at the slag–metal reaction interface, there is partial pressure of CO. When the carbon-saturated metal droplet comes in contact with slag, partial pressure of CO could be taken as partial pressure of CO at the slag–metal reaction interface level and it can be taken as ~ 101,325 Pa. Some researchers [4, 24] also supposed P_{CO} of ~ 101,325 Pa for similar study. Therefore, the oxygen activity can be obtained by using Eqs. (11)–(14).

Based on the above equations, the equilibrium sulfur partition ratio can be obtained as follows:

$$\log L_S = \log \frac{w_{(S)}}{w_{[S]}} = \log C_S + \log K_C + \log a_C + \log f_S - \frac{935}{T} + 1.375 \tag{16}$$

In accordance with experimental results at 1500 °C, the equation between L_S and C_S was:

$$\log L_S = 4.819 + \log C_S \tag{17}$$

Table 4 Values of interaction coefficients [4, 13]

e_S^S	e_S^{Si}	e_S^{Mn}	e_S^C	e_S^P	e_C^S	e_C^{Si}	e_C^{Mn}	e_C^C	e_C^P
− 0.028	0.063	− 0.026	0.11	0.29	0.046	0.08	0.012	0.14	0.051

The sulfur distribution ratio between slag and carbon-saturated iron is measured in the high level of Al_2O_3 in the range of 27.61–40.00 wt.%. The CaO/SiO_2 ratio was between 0.8 and 1.1, and MgO was in the range of 8–16 wt.%. The experimental results are listed in Table 5.

3.3 Effects of CaO/SiO_2 and $(CaO + MgO)/SiO_2$ on L_S

Figure 4a shows the effects of CaO/SiO_2 on sulfur distribution ratio with 11.13 wt.% MgO and 27.61 wt.% Al_2O_3 at 1500 °C. It can be observed that the L_S value increases from 24.29 to 65.38 with increasing the CaO/SiO_2 ratio from 0.8 to 1.1. Figure 4b shows the variations in the effects of CaO/SiO_2 on L_S in $CaO–SiO_2–MgO–Al_2O_3$ slag systems at 1500 °C. As illustrated in Fig. 4b, the results obtained by Zhang et al. [13] and Talapaneni et al. [4] are plotted for comparison. It can be seen from Fig. 5 that the effect of $(CaO + MgO)/SiO_2$ ratio on the distribution ratio is similar to that of CaO/SiO_2 ratio. It is evident that the L_S increases with the increase in CaO/SiO_2 or $(CaO + MgO)/SiO_2$ at fixed Al_2O_3 content and MgO content. The increase in CaO/SiO_2 ratio or $(CaO + MgO)/SiO_2$ causes the disintegration of the silicate network structure, an increase in the proportions of free oxygen ions O^{2-}, CaO, and Ca^{2+}, and then the decrease in $\gamma_{S^{2-}}$ [8, 13]. This indicated that the concentration of free O^{2-} and $\gamma_{S^{2-}}$ have strong effects on the desulfurization process, and a high concentration of free O^{2-} and a low value of $\gamma_{S^{2-}}$ promote the desulfurization performance.

3.4 Effects of Al_2O_3 on L_S

Figure 6a shows the effects of Al_2O_3 on L_S at a fixed CaO/SiO_2 ratio of 0.9 and MgO content of 11.13 wt.%. It can be seen that the L_S value slightly decreases from 24.71 to 22.31 with increasing the Al_2O_3 concentration from 27.61 to 40.00 wt.%. As shown in Fig. 6b, the Al_2O_3 content has a significant effect on the L_S when the Al_2O_3 content in slag is below 20 wt.%. In this case, Al_2O_3 behaves as acidic oxides, and Al^{3+} ions in the slag combine with O^{2-} ions to form AlO_4^{5-} ions like a complex silicate network. As Al_2O_3 increases, the Ca^{2+} in the slag acts as a charge compensation ion and forms $[Ca_{0.5}(AlO_4)]^{4-}$. This leads to the decrease in free O^{2-} [4]. According to the $CaO–SiO_2–MgO–Al_2O_3$ phase diagrams, the increasing Al_2O_3 content causes the formation of complex compounds with high melting points, such as spinel, thus worsening the kinetic condition for desulfurization.

3.5 Effects of MgO on L_S

Figure 7a shows the dependence of L_S on the MgO content in the $CaO–SiO_2–MgO–Al_2O_3$ slag system at a fixed CaO/SiO_2 ratio of 0.9 and Al_2O_3 content of 27.61 wt.% at 1500 °C. The experimental results show that the L_S increases from 22.00 to 43.50 with increasing the MgO content from 8.00 to 16.00 wt.%. Correspondently, it can also be seen from Fig. 7b that the L_S increases with increasing the MgO content at fixed CaO/SiO_2 ratio and Al_2O_3 content in different $CaO–SiO_2–MgO–Al_2O_3$ slag systems. This indicates that MgO has a similar effect as CaO on the desulfurization ability of slag [26]. MgO is well-known to behave as basic oxides and provide O^{2-}, which can promote the desulfurization process. Also, it is observed from the different experimental results that CaO/SiO_2 ratio has a greater effect on L_S than MgO content. This is due to the fact that CaO has a higher optical basicity value (1.00) than MgO (0.78), and CaO could contribute more free O^{2-} ions than MgO in the slag [4]. Therefore, MgO shows less effect on desulfurization ability than CaO.

Table 5 Experimental data and sulfur distribution ratio of different slag compositions at 1500 °C

No.	CaO/wt.%	SiO_2/wt.%	MgO/wt.%	Al_2O_3/wt.%	CaO/SiO_2	$w_{(S)}$/wt.%	$w_{[S]}$/wt.%	L_S	logC_S
1	27.23	34.03	11.13	27.61	0.8	0.85	0.035	24.29	− 3.43
2	29.02	32.24	11.13	27.61	0.9	0.84	0.034	24.71	− 3.43
3	30.63	30.63	11.13	27.61	1.0	0.84	0.018	46.67	− 3.15
4	32.09	29.17	11.13	27.61	1.1	0.85	0.013	65.38	− 3.00
5	30.50	33.89	8.00	27.61	0.9	0.77	0.035	22.00	− 3.48
6	26.71	29.68	16.00	27.61	0.9	0.87	0.02	43.50	− 3.18
7	25.52	28.35	11.13	35.00	0.9	0.86	0.033	26.06	− 3.40
8	23.15	25.72	11.13	40.00	0.9	0.87	0.039	22.31	− 3.47

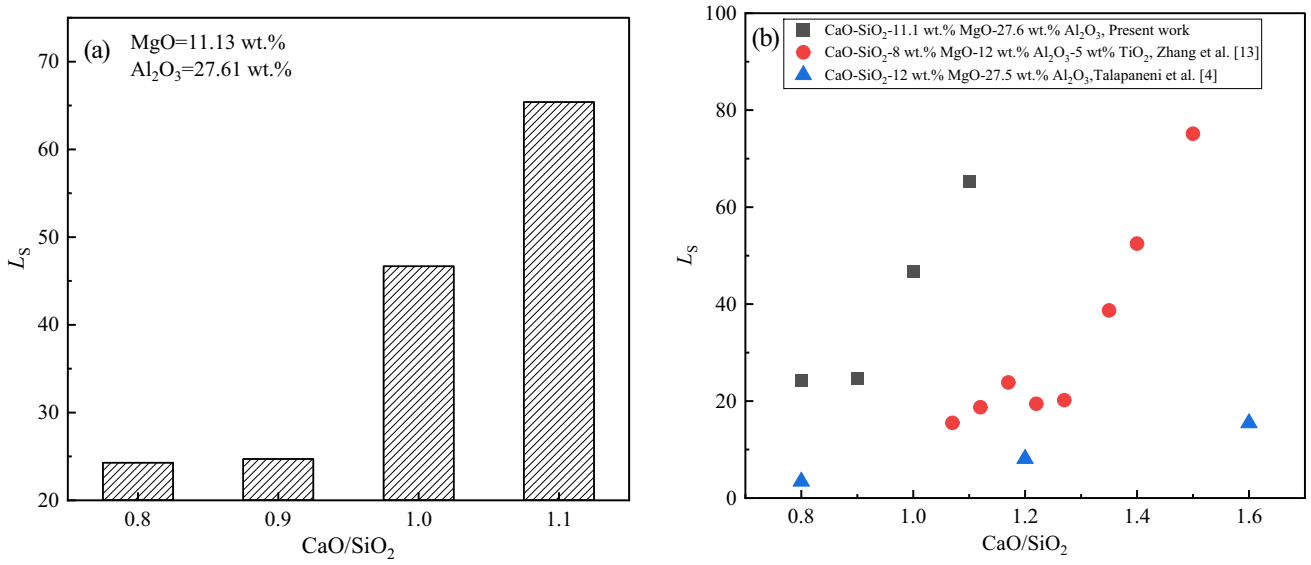

Fig. 4 Effect of CaO/SiO_2 on L_S at 1500 °C (**a**) and variations in effect of CaO/SiO_2 on L_S in $CaO–SiO_2–MgO–Al_2O_3$ slag systems at 1500 °C (**b**)

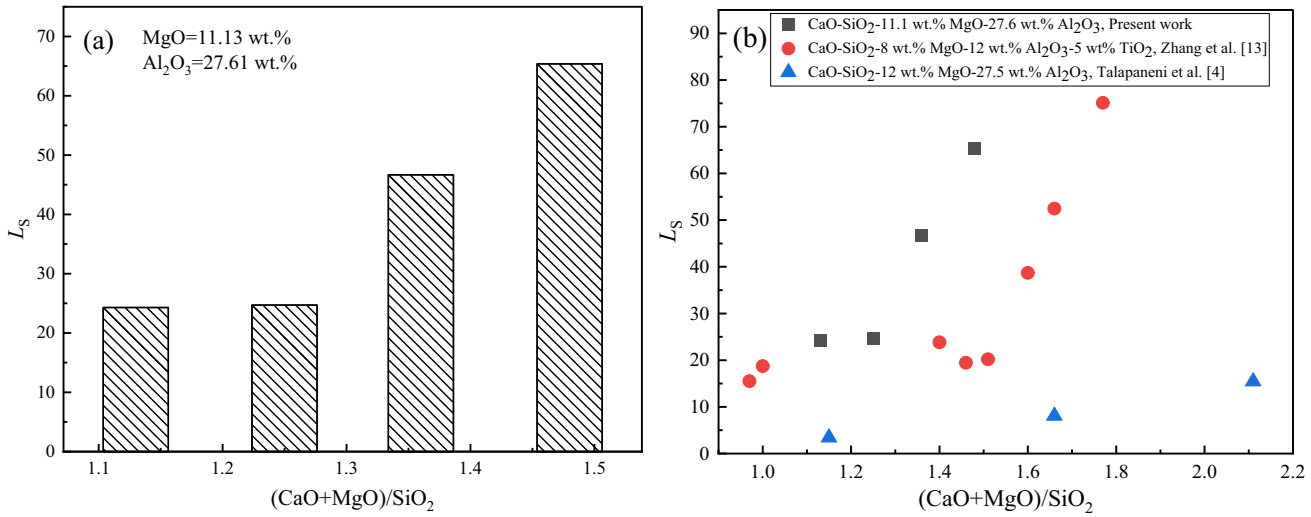

Fig. 5 Effect of $(CaO + MgO)/SiO_2$ on L_S at 1500 °C (**a**) and variations in effect of $(CaO + MgO)/SiO_2$ on L_S in $CaO–SiO_2–MgO–Al_2O_3$ slag systems at 1500 °C (**b**)

3.6 Microstructure and phase analysis

Figure 8 shows the SEM–EDS images of desulfurization slag. It can be seen that the main phases contain light-gray silicate with high calcium and low magnesium, dark-gray silicate with high magnesium and low calcium, black spinel, and white ferrochrome. The sulfur is mainly distributed in the silicate phase and almost absent in the spinel phase and ferrochrome alloys. The EDS image can prove that the calcium ions and magnesium ions combine with sulfur ions to form ionic clusters, which promote the desulfurization reaction.

3.7 Comparison with sulfide capacity models

The experimentally determined sulfide capacities in the present study are compared with that calculated by different models in Refs. [32–36]. The sulfide capacity models for $CaO–SiO_2–MgO–Al_2O_3$ slag systems are shown in Table 6. Figure 9 shows the effect of corrected optical basicity on sulfide capacities of $CaO–SiO_2–MgO–Al_2O_3$ slag systems at 1500 °C. It is observed that sulfide capacity increases with increasing the corrected optical basicity of slags. The comparisons between predicted and experimentally determined sulfide capacity values for $CaO–SiO_2–MgO–Al_2O_3$ slag systems at 1500 °C are shown in

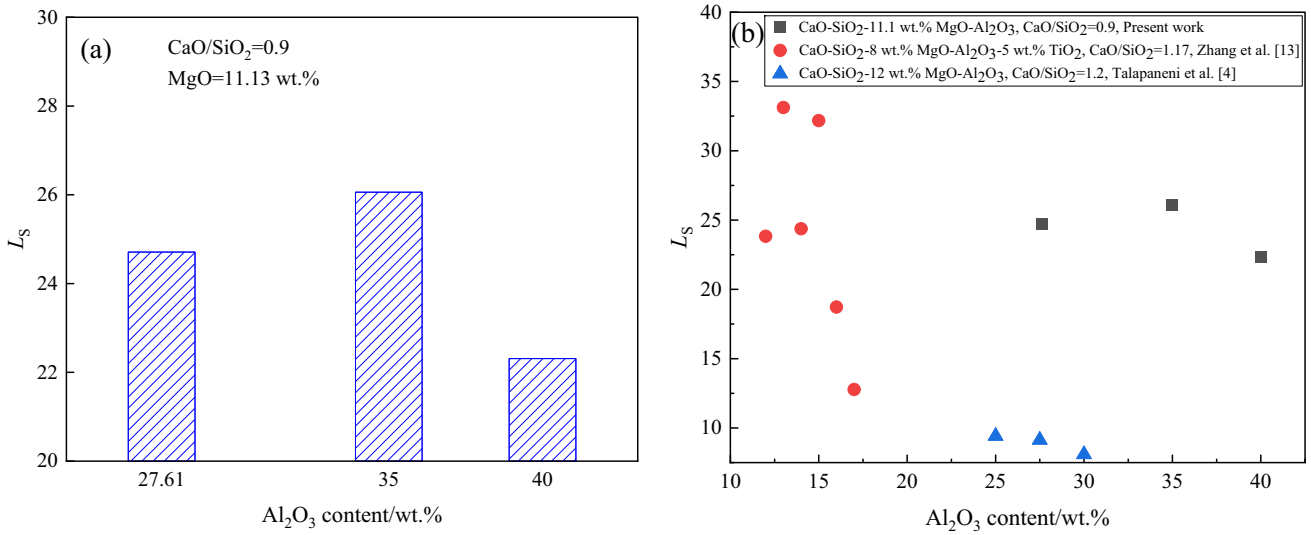

Fig. 6 Effect of Al_2O_3 on L_S at 1500 °C (**a**) and variations in effect of Al_2O_3 on L_S in CaO–SiO_2–MgO–Al_2O_3 slag systems at 1500 °C (**b**)

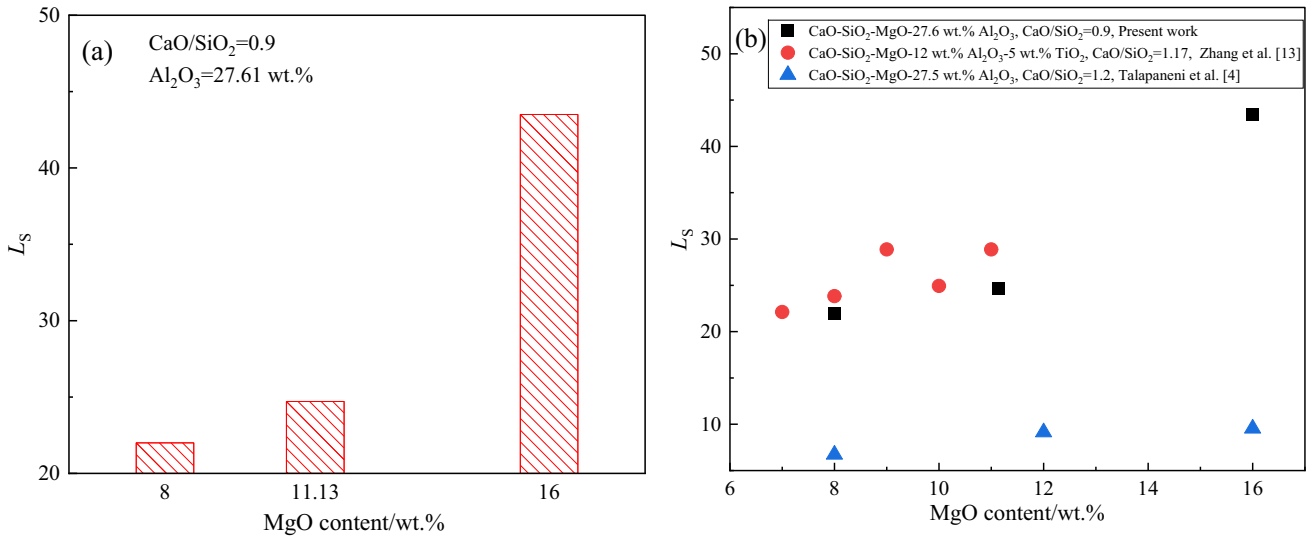

Fig. 7 Effect of MgO on L_S at 1500 °C (**a**) and variations in effect of MgO on L_S in CaO–SiO_2–MgO–Al_2O_3 slag systems at 1500 °C (**b**)

Fig. 10. It is evident that the sulfide capacity values predicted by Young et al. [36] are much higher than experimentally determined sulfide capacity values, which is also reported by other researchers [32, 34], while the models of Zhang et al. [32], Sosinsky and Sommerville [33], Hao and Wang [34], and Ren et al. [35] underpredict the sulfide capacity values. This may be because the above-mentioned models are based on optical basicity or corrected optical basicity and take no account of the effects of charge compensation of Ca^{2+} to $[AlO_4]^{5-}$ on sulfide capacity.

4 Conclusion

The effects of MgO, Al_2O_3, and CaO/SiO_2 ratio on the liquid areas of the CaO–SiO_2–MgO–Al_2O_3 slag were predicted thermodynamically using FactSage 8.0 software, and then the effects of MgO, Al_2O_3, and CaO/SiO_2 on the sulfur distribution ratio between CaO–SiO_2–MgO–Al_2O_3 slag with high alumina and carbon-saturated iron were investigated via slag–metal equilibrium technique at 1500 °C. The liquid areas of CaO–SiO_2–MgO–Al_2O_3 slag decreased with increasing Al_2O_3 content. Also, the L_S increased with higher MgO content and higher CaO/SiO_2 ratio largely due to the increase in free O^{2-} icons and the decrease in $\gamma_{S^{2-}}$ in slag, but slightly decreased with increasing Al_2O_3 content because of the decrease in free

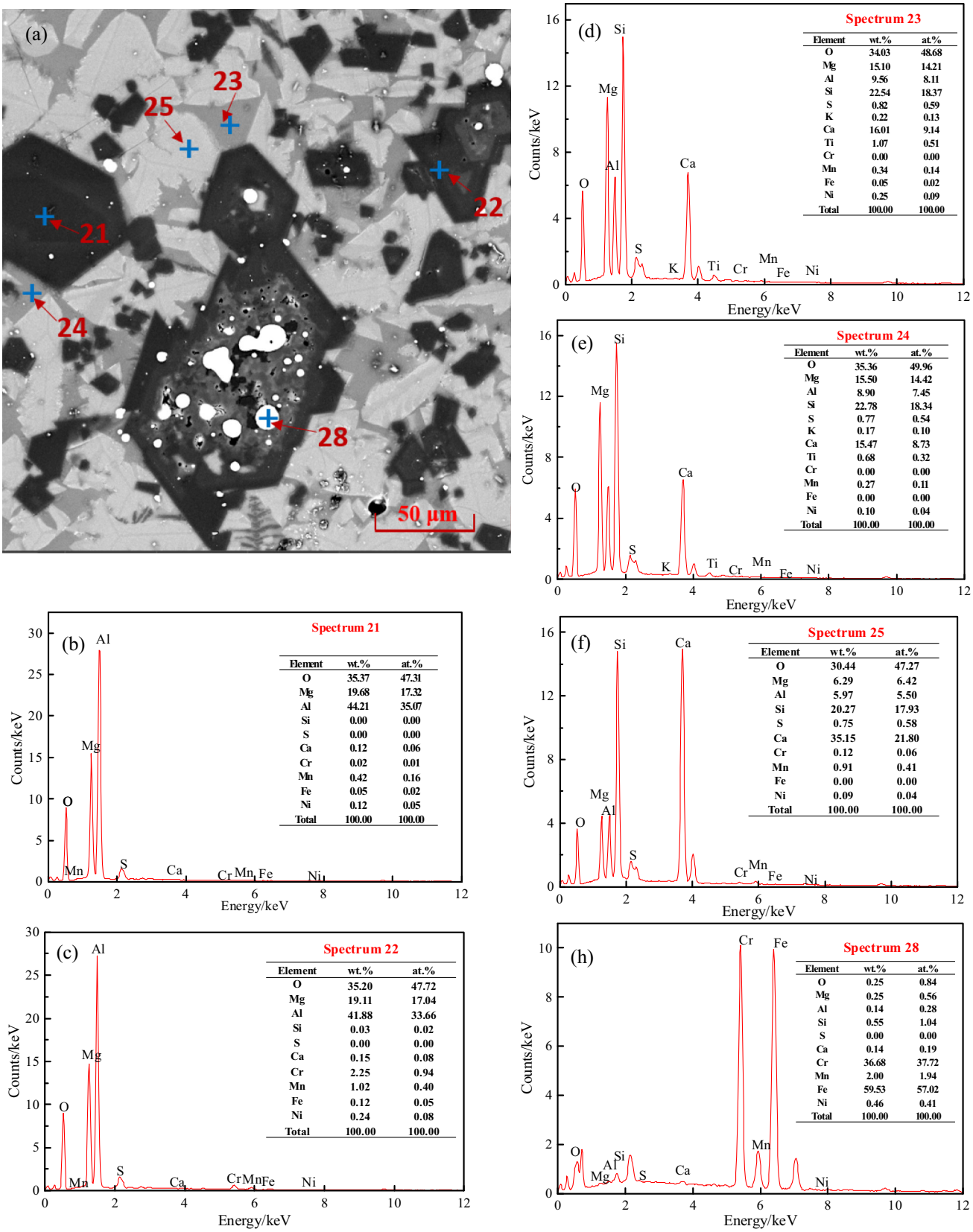

Fig. 8 SEM–EDS images of desulfurization slag

Table 6 Sulfide capacity for $CaO–SiO_2–MgO–Al_2O_3$ slag systems

Authors	Equations
Zhang et al. [32]	$\log C_S = -6.08 + 4.49/\Lambda + (15,893 - 15,864/\Lambda)/T$
Sosinsky and Sommerville [33]	$\log C_S = (22,690 - 54,640\Lambda)/T + 43.6\Lambda - 25.2$
Hao and Wang [34]	$\log C_S = (12,410/\Lambda^{corr} - 27,109)/T + 19.45 - 11.85/\Lambda^{corr}$
Ren et al. [35]	$\log C_S = (-47,236.6 + 52,273.7\Lambda^{corr})/T - 19.46\Lambda^{corr} + 16.89$
Young et al. [36]	$\log C_S = -13.913 + 42.84\Lambda - 23.82\Lambda^2 - 11,710/T - 0.02223X_{SiO_2} - 0.02275X_{Al_2O_3}$

Λ—Optical basicity; Λ^{corr}—corrected optical basicity; X_{SiO_2}—mole fraction of SiO_2 in slag; $X_{Al_2O_3}$—mole fraction of Al_2O_3 in slag

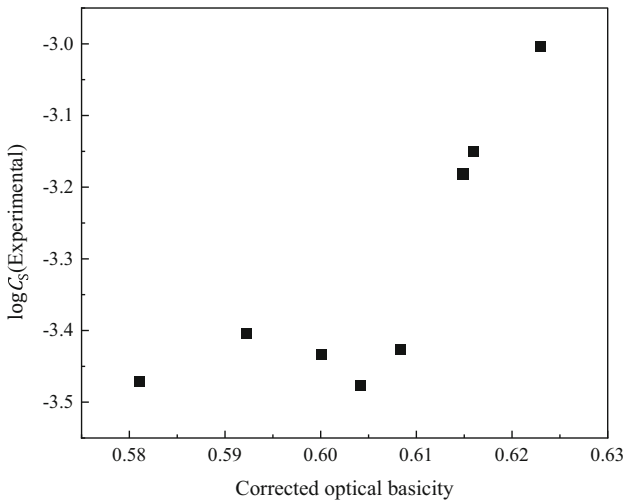

Fig. 9 Effect of corrected optical basicity on sulfide capacities of $CaO–SiO_2–MgO–Al_2O_3$ slag systems at 1500 °C

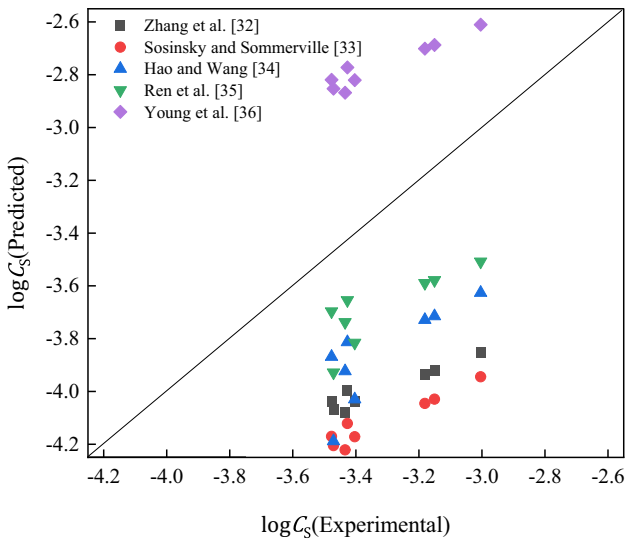

Fig. 10 Comparison between predicted and experimentally determined sulfide capacity values for $CaO–SiO_2–MgO–Al_2O_3$ slag systems at 1500 °C

O^{2-}. Besides, MgO showed less effect on desulfurization ability than CaO.

Acknowledgements The authors gratefully acknowledge the support from the National Natural Science Foundation of China Project (52104345) and the Major Science and Technology Special Project of Yunnan Province (202002AB080001-1).

Declarations

Conflict of interest The authors declare that they have no known competing financial interests or personal relationships that could have appeared to influence the work reported in this paper.

References

[1] J. Yang, M. Kuwabara, T. Sakai, N. Uchida, Z. Liu, M. Sano, ISIJ Int. 47 (2007) 418–426.
[2] D. Roy, P.C. Pistorius, R.J. Fruehan, Metall. Mater. Trans. B 44 (2013) 1086–1094.
[3] W. Ma, H. Li, Y. Cui, B. Chen, G. Liu, J. Ji, ISIJ Int. 57 (2017) 214–219.
[4] T. Talapaneni, N. Yedla, S. Sarkar, Metall. Res. Technol. 115 (2018) 502.
[5] R. de Oliveira Pezzin, A.P.L. Berger, F.F. Grillo, E. Junca, H.S. Furtado, J.R. de Oliveira, J. Mater. Res. Technol. 9 (2020) 838–846.
[6] M.Y. Mohassab-Ahmed, H.Y. Sohn, H.G. Kim, Ind. Eng. Chem. Res. 51 (2012) 3639–3645.
[7] P.K. Iwamasa, R.J. Fruehan, Metall. Mater. Trans. B 28 (1997) 47–57.
[8] X. Ma, M. Chen, H. Xu, J. Zhu, G. Wang, B. Zhao, ISIJ Int. 56 (2016) 2126–2131.
[9] C.J.B. Fincham, F.D. Richardson, Proc. R. Soc. Lond. A 223 (1954) 40–62.
[10] K. Zhang, Y. Zhang, T. Wu, Metals 8 (2018) 1068.
[11] S.R. Simeonov, I.N. Ivanchev, A.V. Hainadjiev, ISIJ Int. 31 (1991) 1396–1399.
[12] N.M. Anacleto, H.G. Lee, P.C. Hayes, ISIJ Int. 33 (1993) 549–555.
[13] J. Zhang, X. Lv, Z. Yan, Y. Qin, C. Bai, Ironmak. Steelmak. 43 (2016) 378–384.
[14] Z. Yan, X. Lv, J. Zhang, Y. Qin, C. Bai, Can. Metall. Quart. 55 (2016) 186–194.
[15] L. Yao, S. Ren, X. Wang, Q. Liu, L. Dong, J. Yang, J. Liu, Steel Res. Int. 87 (2016) 241–249.
[16] C.K. Du, J. Yang, X.Z. Zhao, Y.J. Shi, J.L. You, X.D. Gao, J. Iron Steel Res. 25 (2013) No. 7, 19–22.

[17] C.Y. Xu, C. Wang, R.Z. Xu, J.L. Zhang, K.X. Jiao, Int. J. Miner. Metall. Mater. 28 (2021) 797–803.
[18] T. Zhang, H. Zhang, S. Dai, D. Huang, W. Wang, Ceram. Int. 47 (2021) 22918–22923.
[19] S.S. Biswal, C. Panda, S. Sahoo, T. Jena, K.C. Panda, Mater. Today Proc. 35 (2021) 97–101.
[20] H. Zheng, Y. Ding, Q. Wen, S. Zhao, X. He, S. Zhang, C. Dong, Sci. Total Environ. 802 (2022) 149830.
[21] L. Deng, X. Zhang, M. Zhang, X. Jia, J. Non-Cryst. Solids 500 (2018) 310–316.
[22] K.D. Kim, W.W. Huh, D.J. Min, Metall. Mater. Trans. B 45 (2014) 889–896.
[23] J.S. Han, J.G. Kang, J.H. Shin, Y. Chung, J.H. Park, Ceram. Int. 44 (2018) 13197–13204.
[24] A. Shankar, M. Gornerup, S. Seetharaman, A.K. Lahiri, Metall. Mater. Trans. B 37 (2006) 941–947.
[25] J.F. Xu, J.Y. Zhang, C. Jie, L. Tang, K. Chou, Adv. Mater. Res. 194–196 (2011) 169–174.
[26] Y. Taniguchi, N. Sano, S. Seetharaman, ISIJ Int. 49 (2009) 156–163.
[27] W.H. Van Niekerk, R.J. Dippenaar, ISIJ Int. 33 (1993) 59–65.
[28] Y. Park, D.J. Min, ISIJ Int. 56 (2016) 520–526.
[29] J. Tang, M. Chu, C. Feng, Y. Tang, Z. Liu, ISIJ Int. 56 (2016) 210–219.
[30] T. Jiang, S. Wang, Y. Guo, F. Chen, F. Zheng, Metals 6 (2016) 107.
[31] X.H. Huang, Principles of steel metallurgy, 4th, Metallurgical Industrial Press, Beijing, China, 2020.
[32] G.H. Zhang, K.C. Chou, U. Pal, ISIJ Int. 53 (2013) 761–767.
[33] D.J. Sosinsky, I.D. Sommerville, Metall. Trans. B 17 (1986) 331–337.
[34] X. Hao, X. Wang, Steel Res. Int. 87 (2016) 359–363.
[35] Z.S. Ren, X.J. Hu, K.C. Chou, J. Iron Steel Res. Int. 20 (2013) No. 9, 21–25.
[36] R.W. Young, J.A. Duffy, G.J. Hassall, Z. Xu, Ironmak. Steelmak. 19 (1992) 201–219.